



ELSEVIER

Contents lists available at ScienceDirect

## Thin Solid Films

journal homepage: [www.elsevier.com/locate/tsf](http://www.elsevier.com/locate/tsf)

## Uniaxial magnetic anisotropy in three-bilayer Co/Cu and Co/Al superlattices

Yaobiao Xia<sup>a</sup>, Timothy Yoo<sup>a</sup>, Yu Xiang<sup>a</sup>, Yanli Zhang<sup>b</sup>, Jiyeon Jessica Kim<sup>b</sup>, Tung-Sheng Kuan<sup>b</sup>, Gwo-Ching Wang<sup>a,\*</sup><sup>a</sup> Department of Physics, Applied Physics and Astronomy, Rensselaer Polytechnic Institute, 110, 8th Street, Troy, NY 12180-3590, USA<sup>b</sup> Department of Physics, University at Albany, State University of New York, 1400 Washington Avenue, Albany, NY 12222, USA

## ARTICLE INFO

## Keywords:

Ultrathin superlattices  
Co  
Cu  
Al  
X-ray reflectivity  
Hysteresis loops  
Uniaxial anisotropy  
Anisotropic magnetoresistance

## ABSTRACT

We present the magnetic properties of three-bilayer superlattices  $[\text{Co}(0.8 \text{ nm})/\text{Cu}(1.1 \text{ nm})]_3$  and  $[\text{Co}(0.8 \text{ nm})/\text{Al}(2.2 \text{ nm})]_3$  grown by magnetron sputter deposition on  $\text{SiO}_2$  substrates. Using the surface magneto-optical Kerr effect we observed longitudinal magnetic hysteresis loops with low coercivity values of  $< 17 \times 10^{-4} \text{ T}$  and  $< 7 \times 10^{-4} \text{ T}$  from Co/Cu and Co/Al superlattices, respectively. From the hysteresis loops as a function of in-plane azimuthal angle of the Co/Cu and Co/Al superlattices, we observed an in-plane uniaxial anisotropy in coercivity and squareness. Using a four-point square configuration we observed positive and negative anisotropic magnetoresistances (AMR) with values  $+0.5\%$  and  $-0.5\%$  from Co/Cu superlattice depending on whether the applied current is perpendicular or parallel to the applied magnetic field direction, respectively. The surface morphology including vertical root-mean-square roughness and lateral correlation length were examined by atomic force microscopy. The number of bilayers and the thicknesses of Co, Cu and Al in the superlattices were examined by X-ray reflectivity. The observed magnetic properties were correlated to the interface roughness and layer thickness. The low coercivity, low saturation field, near-one squareness, and finite MR value of the three-bilayer Co/Cu superlattice has potential applications in low magnetic field detection and sensors.

## 1. Introduction

Magnetic superlattices and multilayers (these two terms have been used interchangeably in the literature) have been actively studied since 1980s and peaked in 1990s. The magnetic superlattice consists of repeated bilayers. Each bilayer has an ultrathin ferromagnetic (Fe, Co, Ni, etc.) layer and a non-magnetic spacer layer (Cu, Pd, Cr, etc.). The number of repeated bilayers ( $n$ ) ranges from 5 to 75. The typical thickness of a spacer layer or magnetic layer ranges from about 1 nm to 2 nm [1]. The reduced dimension and confined configuration possess rich quantum phenomena such as oscillatory interlayer coupling and giant magnetoresistance (GMR) [2–4]. The magnetoresistance (MR), coercivity  $H_c$ , and saturation magnetic field  $H_s$  are a function of the spacer layer thickness, which is typically set between 0.5 and 3.5 nm [4,5] depending on the spacer materials in the superlattice [2]. Previous studies have observed that the magnetoresistance MR and  $H_s$  values peak at a certain spacer layer thickness. For example, the Cu spacer layer thicknesses are  $\sim 0.8 \text{ nm}$  and  $\sim 2 \text{ nm}$  for the first and second antiferromagnetic interlayer couplings, respectively, in the Co/Cu superlattice and the MR and  $H_s$  have maximum values [4,6,7]. Straying away from these spacer layer thicknesses results in a decrease

in the observed MR value. As an application example, the GMR reading head device has been applied in commercial disk drives [8]. In recent years, more complicated magnetic superlattice structures have continued to enrich this field where the transition metals are replaced by semiconductors, oxides, and topological insulators [9].

Many early magnetic superlattices were grown by molecular beam epitaxy (MBE) in ultrahigh vacuum ( $10^{-8}$  or  $10^{-9} \text{ Pa}$ ) which allows superior control of the individual layer thickness using a low deposition rate of  $\sim 0.1 \text{ nm/s}$  [8]. The substrate used was often a single crystal, for example, GaAs(001) [8] or Si(001) [3,4] to guide the growth of the crystalline magnetic superlattice for several tens of repeated bilayers. The magnetic signal is known to be proportional to the number of bilayers, as in the GMR value increases with the bilayer number  $n$  [5].

Historically, Co/Cu superlattices, especially those with large  $n$  have been studied extensively. Depending on the deposition methods used, the microstructures of Co/Cu superlattices and their magnetic properties have differed correspondingly. Some works report interfacial structural characterization only [10,11]. Only limited works discuss the effects of structural disorder on the magnetic property [5,12].

In contrast to the Co/Cu superlattice, the Co/Al superlattice has been rarely studied. Prior Co/Al superlattices have been deposited by

\* Corresponding author.

E-mail address: [wangg@rpi.edu](mailto:wangg@rpi.edu) (G.-C. Wang).<https://doi.org/10.1016/j.tsf.2019.04.048>

Received 15 December 2018; Received in revised form 17 March 2019; Accepted 29 April 2019

Available online 30 April 2019

0040-6090/© 2019 Elsevier B.V. All rights reserved.

electron beam deposition [13] and planar magnetron sputtering [14]. Results of structural and magnetic properties observed from these two deposition methods differ greatly. For example, X-ray diffraction analysis revealed that CoAl compound was formed in the e-beam deposited superlattice film [13], but the formation of CoAl compound was not observed from the transmission electron diffraction rings of the sputter deposited film [14]. This is probably due to the fact that the CoAl(110) spacing is very close to the Co(0002) spacing, which makes them indistinguishable from each other in the transmission electron diffraction pattern.

In this work, metallic bilayers were deposited on amorphous SiO<sub>2</sub> on Si(100) substrates by magnetron sputter deposition in a high vacuum. We report the study of the room temperature magnetic properties of Co/Cu and Co/Al superlattices by pushing the repeated number of bilayer down to  $n = 3$ , which is an unexplored superlattice and the individual Co layer thickness to 0.8 nm. The total thickness of the three-bilayer Co/Cu superlattice of  $\sim 7$  nm is the thinnest superlattice that we are aware of. Because the superlattice is ultrathin, conventional structural characterization techniques such as TEM and X-ray diffraction cannot be easily adopted to experimentally study the surface, interface roughness, interface alloying, space layer thickness and grain size. We were able to use the Fourier transform of small angle X-ray reflectivity to obtain the period and number of bilayer of our superlattice without elaborated sample preparation. For surface roughness we used height-height correlation analysis of the AFM images to extract the vertical roughness and lateral correlation length. For magnetic study we measured the hysteresis loop using MOKE as a function of azimuthal angle and experimentally realized the in-plane uniaxial anisotropy. The magnetoresistance was measured using a spring-loaded pin type four-point probe that will not punch through the ultrathin contacts and we observed an anisotropic magnetoresistance with a low saturation field. Then we were able to correlate the roughness and magnetic anisotropy properties. We report new findings from the three-bilayer superlattices and address the question on the effects of structural disorder on the magnetic properties.

The findings include: (1) unusually low coercivity  $< 17 \times 10^{-4}$  T and  $< 7 \times 10^{-4}$  T in Co/Cu and Co/Al superlattices, respectively, compared to that of ultrathin pure Co films of the same thickness; (2) high squareness value (close to 1) along the easy axis direction in both superlattices; (3) an in-plane uniaxial anisotropy of coercivity and squareness for both superlattices; and (4) an in-plane anisotropic magnetoresistance (AMR) of Co/Cu that has a low saturation field and a small but reproducible positive transverse MR value +0.5% and a negative longitudinal MR value of -0.5%. The positive and negative MR directions are along the hard and easy axes directions, respectively, in the uniaxial anisotropy. Our findings also have practical applications in low coercivity and AMR sensors. Using these ultrathin superlattices in devices would naturally cut down on materials costs and avoid the need for costly crystalline substrates.

## 2. Experimental

### 2.1. Growth of superlattices

The superlattices were grown using a DC magnetron sputter deposition with three sputtering targets (Co, Cu, and Al) in a custom-made high vacuum chamber with a base pressure of  $6.5 \times 10^{-5}$  Pa. The radius of the chamber is 17.8 cm (7 in.). Each metal target has a diameter of 5.08 cm (2 in.) and the adjacent targets are  $\sim 48^\circ$  azimuthally apart. Each target faces the center of the chamber and the distance from each sputtering target to the substrate is 14.5 cm (5.7 in.). A shutter is placed in between each target and the substrate. The shutter can be moved vertically up (opened) or down (closed) to allow flux deposition at normal incidence or blocking the flux. The vertical rotational axis of the substrate holder is positioned at the center of the chamber. The substrate holder is mounted off the center by  $\sim 3.3$  cm. The surface of

the mounted sample in the sample holder is parallel to the rotational axis of the sample holder. After the intended layer had been deposited, for example, Co, the sample holder was rotated  $\sim 48^\circ$  to face a different target, for example, Cu target in order to deposit Cu layer. The process was repeated three times to grow three-layers of Co/Cu or Co/Al superlattice. The square substrate was cut from a 725  $\mu\text{m}$  thick Si wafer with a thermally grown 2.4  $\mu\text{m}$  thick SiO<sub>2</sub> on the top of Si(100). The edge length of the substrate was approximately 2.9 cm. Four Ta contact pads of 0.5 cm diameter and 140 nm thickness with the nearest pad center to center spacing of  $\sim 1.4$  cm were deposited onto four corners of SiO<sub>2</sub> prior to the superlattice growth. These Ta pads serve as contacts for *in situ* measurement of electrical resistance and *ex situ* four-point probe magnetoresistance measurement. A circular aperture of 1.8 cm in diameter was placed above the substrate to limit the exposed circular area that would receive the deposition flux. The flux will not completely cover the four Ta pads. The sputtering conditions (mA/V/W) for Co, Cu and Al used were 200/315/63, 50/260/13, and 200/395/79, respectively. Ar pressure was maintained at  $2.8 \times 10^{-1}$  Pa when the Ar flow into the chamber was kept at 5 sccm. The deposition rate of each element was calibrated by *ex situ* AFM step height difference between the test film (deposited for 15 min) and the substrate. For example, a 15 min deposition of Cu film has a height difference of  $\sim 29$  nm in the AFM image. The ratio of height difference over the deposition time gives a deposition rate of Cu  $\sim 1.9$  nm/min. For Co, Cu and Al depositions, the rates were  $2.3 \pm 0.1$ ,  $1.9 \pm 0.1$ , and  $3.9 \pm 0.2$  nm/min, respectively. A 1.5 or 1.6 nm thick Co seed layer was deposited on SiO<sub>2</sub>/Si(100) substrate before the growth of the superlattice. The superlattices grown at room temperature were [Co(0.8 nm)/Cu(1.1 nm)]<sub>3</sub>Co(1.6 nm)/SiO<sub>2</sub>/Si(100) with a total thickness of  $\sim 7$  nm and [Co(0.8 nm)/Al(2.2 nm)]<sub>3</sub>Co(1.5 nm)/SiO<sub>2</sub>/Si(100) with a total thickness of  $\sim 11$  nm. During the film growth and subsequent annealing, a very small current (1  $\mu\text{A}$ ) was applied along the film so that the *in situ* resistance could be monitored in real time. A thermocouple was mounted on the sample to measure the temperature. The sample was mounted on a ceramic wrapped coil filament heater. The resistance of the coil filament was 25  $\Omega$  and the current used was  $< 1.7$  A. Both superlattices were annealed from room temperature to 300  $^\circ\text{C}$  at a heating rate of 9  $^\circ\text{C}/\text{min}$ , after which the heating current was immediately cut off. Literature reported that annealing of granular Co and Cu alloyed film to high temperatures (600–800 K) increases the Co granule size [15]. The sample was cooled naturally to room temperature after several hours in a  $2.8 \times 10^{-1}$  Pa Ar environment in the vacuum chamber. Both Co/Cu and Co/Al superlattices are stable and the hysteresis loops measured over several months in air are reproducible. Schematics of side views of the Co/Cu and Co/Al superlattices are shown in Fig. 1(a) and (b), respectively.

### 2.2. Atomic force microscopy

The surface morphologies of the terminating layer of the superlattice films were imaged using an atomic force microscopy (AFM, PSI XE100) in the contact mode. The AFM tip ( $\mu\text{mash}$ , DPE18/AIBS) used had a tip radius of  $< 35$  nm, a force constant of 3.5 N/m, and a resonant frequency of 75 kHz.

### 2.3. X-ray reflectivity

X-ray reflectivity scans were obtained using a Bruker D8 Discover X-ray, two-circle diffractometer with a Cu source (Cu K $\alpha$ ,  $\lambda = 1.5405$   $\text{\AA}$ , 40 kV, 40 mA) and a linear detector. The anti-scattering slit and the detector slit were both 0.1 mm in order to achieve the maximum resolution. The distance from the X-ray source to the sample and the sample to the detector are 300 mm. This was equal to the slit extension angle of  $\sim 0.02^\circ$ . The X-ray incident angle was  $2^\circ$  and the step size was 0.01  $^\circ$  with a scan speed of 0.1 s/step.

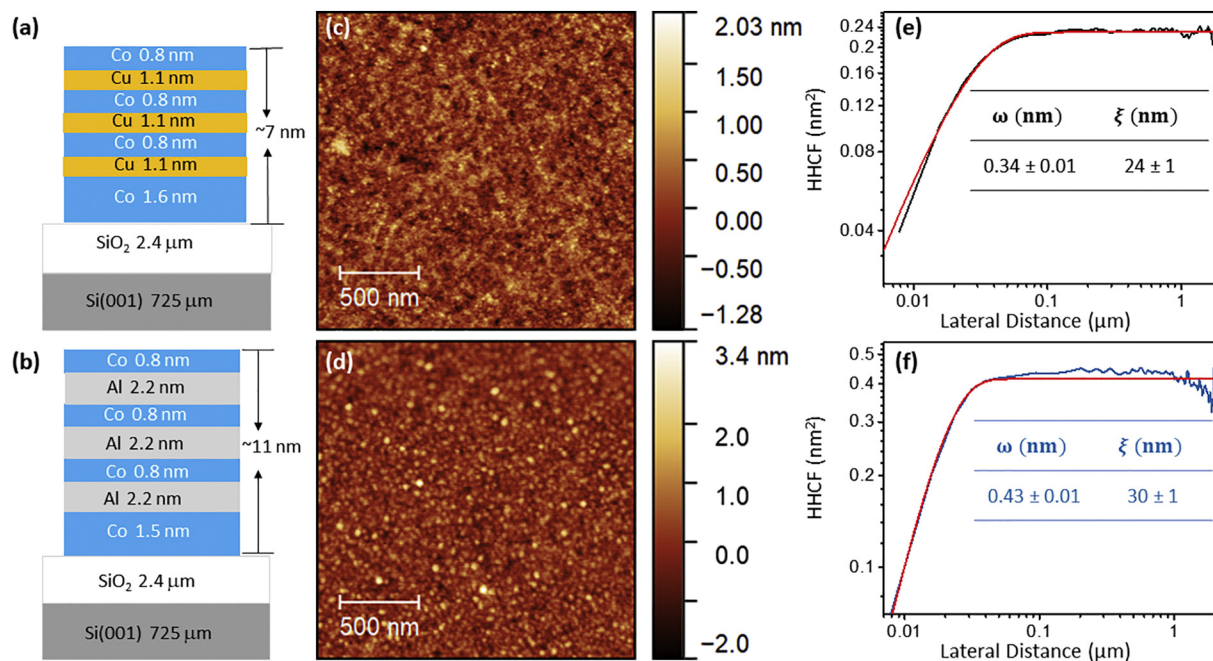


**Fig. 1.** Schematics of (a) Co/Cu and (b) Co/Al three-bilayer superlattices. AFM images (scan size  $2\ \mu\text{m} \times 2\ \mu\text{m}$ ) of top terminating Co surfaces of (c) Co/Cu and (d) Co/Al superlattices. Scale bar is 500 nm. Height-height correlation function analyses of the AFM image of (e) Co/Cu and (f) Co/Al superlattices to extract vertical root mean square roughness  $\omega$  and lateral correlation length  $\xi$ .

#### 2.4. Surface magneto optical Kerr effect

The surface magneto-optical Kerr effect (SMOKE) [16,17] setup was homemade [18,19]. The He-Ne laser source had 10 mW power and 632.8 nm wavelength. We define the x and y directions as the horizontal and into-the-page directions, respectively, while the z direction is in the vertical direction. The longitudinal SMOKE with p polarization was perpendicular to the laser incident plane (x-y plane). The laser was located  $\sim 20$  cm away from the sample, which was placed in the gap of two pole pieces of the electromagnets, in order to avoid any possible effect from the sweeping of the magnetic field. The sweeping of the magnetic field was controlled by a bi-polar power supply. The maximum magnetic field generated by the electromagnet was about  $\pm 0.5$  T. In the measurement of superlattice hysteresis loop the applied field typically used was  $< 10^{-2}$  T due to the low coercivity and saturation magnetic field values of the superlattices. The magnetic field strength was measured using a Hall effect sensor (Honeywell SS94A2D). The applied magnetic field was applied in the x direction and parallel to the sample plane (x-z plane) for the longitudinal SMOKE hysteresis loop measurements. Both the laser incident angle and reflected angle relative to the sample surface normal were  $42^\circ$ . These angles were achieved by using two Ag coated mirrors. The reflected laser light went through an analyzer and into a Si photodetector (Thor Labs FDS1010). The photodiode was connected to a preamplifier, an analog to digital converter (ADC), and then to a PC where a LabView program acquired the data and constructed the hysteresis loop by plotting the Kerr intensity vs. the applied magnetic field. For the in-plane azimuthal magnetic anisotropy study the sample was mounted on a precision rotation stage (Newport 481-A) with the sample plane (x-z plane) parallel to the rotational stage. We defined the azimuthal angle  $\phi = 0^\circ$  as the horizontal or x-direction of the sample plane. The longitudinal SMOKE hysteresis loops were collected at intervals of  $15^\circ$  in-plane azimuthal angle over  $360^\circ$  by rotating the precision stage clockwise in the x-z plane.

#### 2.5. Magnetoresistance

After the SMOKE measurements, the magnetoresistance was

measured using a four-point probe in a square configuration under a sweeping magnetic field. The spring-loaded pin (SPA-1 J, Everett Charles Technologies) was inserted in one end of a receptacle (SPR-1 W, ECT) [19]. Each assembled probe was fitted in one of the four holes at the four corners of a square in an acrylic plate. The spacing between the nearest adjacent probes was  $\sim 1.3$  cm. See the left inset of Fig. 4(a). On the sample surface, four tantalum (Ta) pads which had a nearest neighbor spacing of  $\sim 1.3$  cm were first deposited on the four corners of the  $\text{SiO}_2/\text{Si}$  substrate before the deposition of superlattice described previously. The diameter and the thickness of each Ta pad were  $\sim 0.5$  cm and 140 nm, respectively. The superlattice sample placed vertically on an Aluminum plate (in the x-z plane) in the gap of the two pole pieces of the electromagnet (the same magnet used for SMOKE measurements). The four spring-loaded probes were moved to gently touch the Ta pads using a linear micrometer. The applied magnetic field was directed parallel to the plane of the sample in the x-direction, while the applied current was either perpendicular or parallel to the applied magnetic field direction. The applied current (Keithley 2400) in two contact probes was typically in the range of tens of mA and the voltage (Keithley 182) measured from another two contact probes was typically in the range of sub volts. The voltage vs. applied magnetic field was measured and then the voltage was converted to the resistance by dividing the measured voltage by the applied current.

### 3. Results and discussion

We first present quantitative surface and interfacial structural characterization followed by the magnetic measurements. The magnetic properties affected by the structural disorder are discussed in the relevant sections.

#### 3.1. Morphology and roughness of top terminating Co layer

The surface morphologies of the Co/Cu and Co/Al superlattices were imaged in air by AFM immediately after the superlattice growth and anneal. These images of Co/Cu and Co/Al are shown in Fig. 1(c) and (d), respectively. The corresponding height-height correlation

function (HHCF) analyses [20,21] of the AFM images are shown in Fig. 1(e) and (f), respectively. It is noted that the surface features observed represent the oxidized surface of the top Co layer. Nevertheless, they reflect the overall smoothness of the original Co surface. The Co terminating surfaces have their root-mean-square roughness (RMS)  $\omega$  in the sub-nm range. The  $\omega$  values for Co/Cu and Co/Al superlattices are 0.34 and 0.43 nm, respectively. These numbers indicate that the smoothness of the top terminating layer is in the range of a couple of atomic layer thickness. The lateral correlation lengths  $\xi$  measured for the Co/Cu and Co/Al superlattices are  $24 \pm 1$  and  $30 \pm 1$  nm, respectively. Co and Cu are mutually immiscible and in principle are expected to grow conformally and form sharp interfaces. In practice, the growth of Co on Cu or Cu on Co may form island-like features that we observed from the AFM images. Besides the roughness, the Co and Cu layers are polycrystalline when grown by e-beam [5] or sputtering [10]. As a comparison of the lateral correlation length of Co/Cu superlattice, our tens of nm is comparable to the polycrystalline grain size of 10–14 nm observed in the Co(1.5 nm)/Cu(0.8 nm)]<sub>8</sub> superlattice grown by e-beam evaporation [5] and upper limit of 25 nm grain size estimated from superlattice [Co(1.5 nm)/Cu(0.9 nm)]<sub>40</sub> grown by DC magnetron sputtering [22] but is larger than the reported 1.7 nm determined from the magnetron-sputtered Si(001)/[Co(1.2 nm)/Cu(0.97 nm)]<sub>30</sub>/(Cu 3 nm) superlattice with  $n = 30$  [10].

The magnetic measurements were performed *ex situ*. We expect that the terminating Co surface is not pure Co. An oxidation study of Co/Cu multilayer reported that for a short time after the deposition, the oxidation layer is a constant and the thickness is  $< 1$  nm. However, for a long time after the deposition, the thickness of oxide layer is proportional to the original Co layer thickness. For a 0.9 nm thick Co layer the oxide layer thickness is about 1 nm and the oxidation seems to have stopped at the Cu/Co interface [23]. Applying this result to our 0.8 nm thick top terminating Co layer of the superlattice Co/Cu, the oxidation should have stopped at the first Cu/Co interface. This halting of oxidation at the first Co/Cu interface means the Co in the superlattice other than the top Co layer will not be oxidized and the pure Co layers underneath will be preserved.

### 3.2. Three-bilayer superlattice examined by X-ray reflectivity

X-ray reflectivity (XRR) can be used to characterize a non-ideal superlattice when coupled with model simulations. Typical parameters extracted are thickness and period of the multilayer. The X-ray reflectivity intensity of each superlattice was measured as a function of small  $2\theta$  angle. The intensities of Co/Cu and Co/Al superlattices are shown in Fig. 2(a) and (b), respectively. A visual inspection of the data show five peaks consistent with Kiessig fringes of  $2n - 1$ , where  $n$  is the number of bilayers [11]. For our superlattice samples,  $n$  is 3. This  $2\theta$  angle has been converted to the reciprocal distance ( $q$ ) using the relations:  $2d\sin\theta = \lambda$  and  $d = \frac{2\pi}{q}$ , where  $d$  is the interlayer spacing. Fig. 2(c) and (d) show X-ray reflectivity as a function of  $q$  for Co/Cu and Co/Al superlattices, respectively. We performed a Fourier transform of the X-ray reflectivity data shown in Fig. 2(c) and (d) in the same way as that mentioned in Bernabe et al.'s work [11] and the corresponding results are shown in Fig. 2(e) and (f), respectively. The insets in Fig. 2(e) and (f) list the peak centers and peak widths.

For the Co/Cu superlattice, peak p1 and peak p2 shown in Fig. 2(e) are located at 0.99 nm and 1.83 nm, respectively. The observed peak p1 at 0.99 nm is close to the average thickness of one Co layer and one Cu layer ( $0.95 \text{ nm} = (0.8 \text{ nm Co} + 1.1 \text{ nm Cu})/2$ ). In principle, from the Fourier transform of the XRR spectrum, we should see individual peaks from Co layer at 0.8 nm and Cu layer at 1.1 nm. In practice, the width of peak p1 is 0.59 nm. If we assume peak p1 is composed of two Gaussian peaks located at 0.8 nm and 1.1 nm with the same width  $w$ , then the width of the two convoluted peaks would be 0.59 nm. Then from  $\sqrt{w^2 + w^2} = 0.59 \text{ nm}$ , one obtains the calculated width  $w$  of an

individual peak to be  $\sim 0.42 \text{ nm}$ , which is larger than their thickness difference ( $0.3 \text{ nm} = 1.1 \text{ nm} - 0.8 \text{ nm}$ ). This explains why the peaks merged together and show up as one peak p1. The p2 peak position at 1.83 nm is about one bilayer of Co/Cu ( $1.9 \text{ nm} = 0.8 \text{ nm Co} + 1.1 \text{ nm Cu}$ ). This depicts that the Co and Cu have a bilayer structure.

For the Co/Al superlattice, peak p3 and peak p4 are located at 1.27 nm and 2.25 nm, respectively. The p3 peak position is close to the average thickness of one Co layer and one Al layer ( $1.5 \text{ nm} = (0.8 \text{ nm} + 2.2 \text{ nm})/2$ ). The p4 peak position is about the thickness of one Al layer. The one bilayer thickness at 3.0 nm ( $= 0.8 \text{ nm} + 2.2 \text{ nm}$ ) is not observed because of the low intensity resulted possibly from the cumulative interfacial roughness and interfacial alloying.

It is estimated that one monolayer CoAl compound was already formed at the Co and Al interfaces during deposition. The binary phase diagram [24] of Co and Al also shows many compound phases formed at room temperature. This means that the total amount of pure Co has been reduced. After annealing the Co/Al superlattice to 300 °C and cooled down to room temperature, the amount of pure Co layer was further reduced. This CoAl alloy formation is consistent with the literature report of 38 repeated bilayers of thicker Co and thicker Al layers, [Co(1 nm)/Al(7 nm)]<sub>38</sub>. This previous report showed a TEM cross section image of Co/Al superlattice that has a layer structure [13]. However, the individual Co layer seems discontinuous. Their TEM diffraction pattern showed Al and CoAl texture rings. From our current study and literature report, that part of the Co has been alloyed with Al, so the individual layer thickness and the total bilayer thickness of Co and Al may not be the same as the intended thickness.

Our XRR results of Co/Cu and Co/Al superlattices indicate that despite the interfacial roughness and interfacial alloying of Co/Al superlattice, the overall three bilayer superlattices are of good quality. The Co/Cu superlattice has a better interfacial quality as compared with that of Co/Al superlattice. This difference in interfacial roughness will reflect in their magnetic properties presented in the next sections.

Our bilayer structure is consistent with the observation from TEM cross sectional views of eight repeated [Co(1.5 nm)/Cu(0.8 nm)]<sub>8</sub> sandwiched between substrate seed Si(100)/Co(6 nm) and top cap layer Co(4.5 nm) [5] and 16 repeated [Co(1 nm)/Cu(0.9 nm)]<sub>16</sub> sandwiched between Si(100)Cu(5 nm) seed layer and Fe(5 nm) cap layer [3] published in the literature. The observed intensity decay and peak broadening may contribute from the interface roughness [11]. The fact that we can observe 5 Kiessig fringes ( $2n-1$ ) in X-ray reflectivity from three-bilayer superlattice implies that the interface roughness is not severe. We can estimate the upper limit of the vertical interface roughness from the root mean square roughness analyzed from the AFM image shown in Fig. 1(a). We assume that the deposition of Co to Cu or Cu on Co are conformal and the interface roughness propagates to the surface. Since the surface RMS is  $0.34 \pm 0.1 \text{ nm}$ , we may approximate the interface roughness to be in the sub nm range.

The TEM selected area diffraction patterns show ring patterns from 40 repeated [Co(1.9 nm)/Cu(1.0 nm)]<sub>40</sub> multilayers [12] and 40 repeated [Co(1.5 nm)/Cu(0.9 nm)]<sub>40</sub> multilayers [22]. These results indicate that the multilayers are polycrystalline. We believe our ultrathin three bilayer superlattice is polycrystalline, since a film grown on an amorphous SiO<sub>2</sub> substrate is known to be polycrystalline.

### 3.3. Azimuthal dependent longitudinal hysteresis loops and in-plane uniaxial anisotropy

We measured the longitudinal hysteresis loops of Co/Cu superlattice by rotating the sample's azimuthal angle every 15° increment. The hysteresis loop changes its shape as the azimuthal angle changes. Fig. 3(a) and (b) show the measured longitudinal hysteresis loops of Co/Cu superlattice along the easy and hard axes directions, respectively. Both H<sub>c</sub> values are  $< 20 \times 10^{-4} \text{ T}$ . The saturation magnetic field H<sub>s</sub> for Kerr intensity or magnetization is  $\sim 100 \times 10^{-4} \text{ T}$ . Recall the

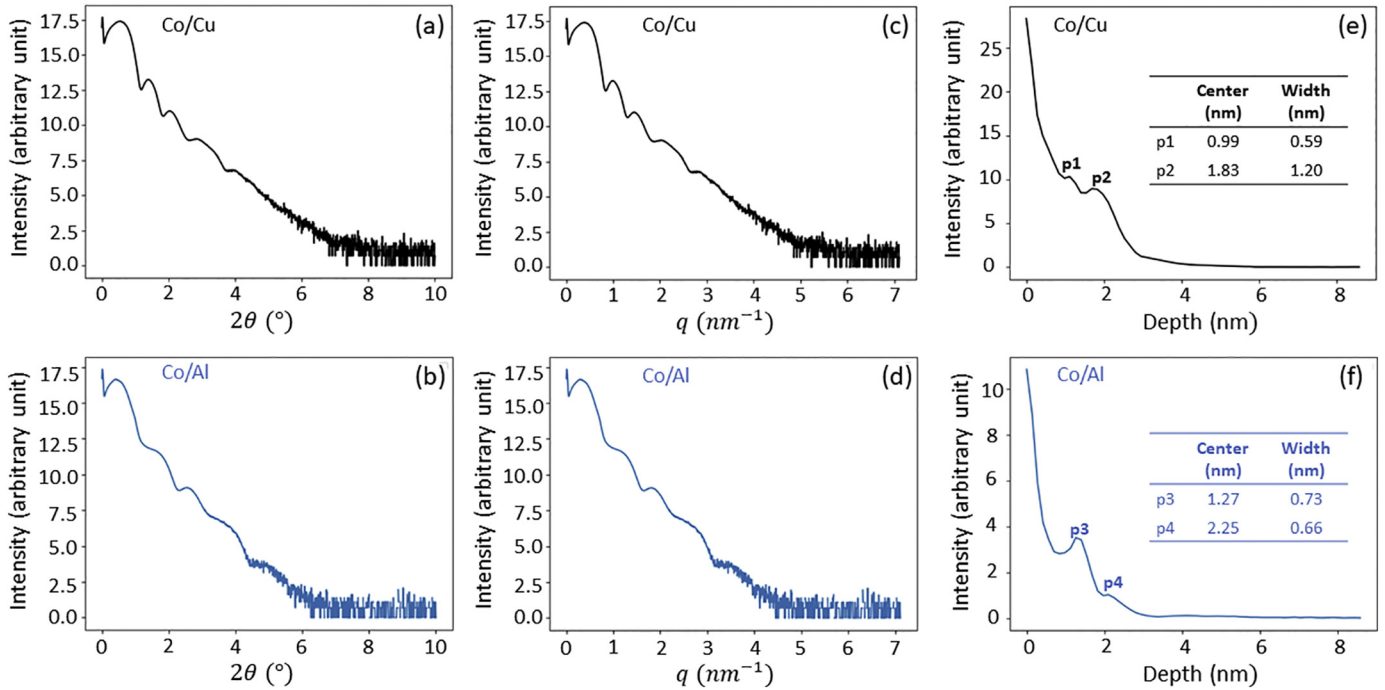


**Fig. 2.** X-ray reflectivity measurements of (a) Co/Cu and (b) Co/Al superlattices plotted in units of  $2\theta$  in the angular range from 0 to  $10^\circ$ . X-ray reflectivity intensities of (c) Co/Cu and (d) Co/Al superlattices plotted in the reciprocal space in units of  $\text{nm}^{-1}$ . Fourier transform of X-ray reflectivity intensities of (e) Co/Cu and (f) Co/Al superlattices vs. depth from the top terminating surface in units of nm.

measured Kerr intensity is proportional to the magnetization [16]. The squareness associated with the loop in the easy axis direction is close to 1. We use the conventional definition of squareness  $S = M_r/M_s$ , where  $M_r$  is remnant magnetization and  $M_s$  is saturation magnetization.

The values of coercivity,  $H_c$ , and squareness,  $S$ , of the Co/Cu superlattice are not constant and depend on the sample's in-plane azimuthal angle. Fig. 3(c) and (d) plot the coercivity and squareness of Co/Cu superlattice over  $360^\circ$  azimuthal angles, respectively. These uniaxial anisotropies in  $H_c$  and squareness are graphically symmetrical. The coercivity value ranges from  $(17.15 \pm 0.50) \times 10^{-4} \text{ T}$  to  $(3.60 \pm 1.20) \times 10^{-4} \text{ T}$ , and the squareness value varies from  $0.96 \pm 0.05$  to  $0.19 \pm 0.03$ . For a loop measured with the applied field along the easy axis of magnetization (Fig. 3(a)), the shape is square-like and the squareness is close to 1. This indicates an abrupt flipping of the magnetization direction within the superlattice. The squareness of the hysteresis loop appears to indicate that the interlayer coupling is ferromagnetic. This is understood by realizing that our Cu spacer layer thickness is  $\sim 1.1 \text{ nm}$  and not the  $\sim 0.8 \text{ nm}$  spacer layer thickness that is most optimal for the first antiferromagnetic coupling in the Co/Cu superlattice [4,6]. Compared with the literature report, the maximum  $H_c$  value of our Co/Cu superlattice is less than the  $35 \times 10^{-4} \text{ T}$  that was observed from Si/Co (6 nm)/[Cu( $t_{\text{Cu}}$ )/Co (1.5 nm)] $_n$ /Co (4.5 nm) multilayers where  $9 < n < 13$  and  $t_{\text{Cu}}$  ranges from 0.7 to 3.5 nm [6]. For the hard-axis loop, the shape is spindle-like, and the squareness is  $< 1$ . This indicates a more gradual transition from one saturated magnetization state to the other.

Besides the magnetic coupling, the  $H_c$  value of Co depends on the Cu substrate's roughness as well as the Co thickness in the ultrathin regime. For instance, the  $H_c$  value for Co film grown by molecular beam epitaxy (MBE) on Cu(001) surface depends on the roughness of the starting Cu(001) surface. If the Cu(001) surface is smooth to start with, then the  $H_c$  value increases from  $\sim 12 \times 10^{-4} \text{ T}$  at 2 ML to  $\sim 60 \times 10^{-4} \text{ T}$  at 6 ML and stays constant as the thickness increases to 30 ML [25], where the monolayer (ML) height is half of the lattice constant, 0.354 nm. Rather, if the starting Cu(001) surface is pre-roughened slightly by *in-situ* ion sputtering with an RMS roughness of 0.1 nm before the Co deposition,

then the  $H_c$  is constant at  $\sim 45 \times 10^{-4} \text{ T}$  from 1 to 6 ML. On the other hand, if the Cu(001) surface is heavily roughened, then the  $H_c$  value is much higher and stays around  $(160 \pm 5) \times 10^{-4} \text{ T}$  from 2 to 6 ML. For reference, the 0.8 nm thick Co in our three-bilayer Co/Cu superlattice is about 4 ML, which corresponds to a coercivity of  $40 \times 10^{-4} \text{ T}$  given that it was grown on a smooth Cu(001) surface. A similar trend in the thickness dependent coercivity of the Co film grown by MBE on Cu(111) surface with Pb surfactant [26] was also observed where  $H_c \sim 80 \times 10^{-4} \text{ T}$  at  $\sim 4 \text{ ML}$  and peaks at  $\sim 120 \times 10^{-4} \text{ T}$  at 6 ML.

Regarding the azimuthal anisotropy of the superlattice, Fig. 3(e) and (f) plot the coercivity and squareness of the Co/Al superlattice over  $360^\circ$  azimuthal angles, respectively. Similar to the Co/Cu case, both  $H_c$  and squareness have two relative maxima and two relative minima about  $180^\circ$  apart over the  $360^\circ$  azimuthal angle. The anisotropy axis is observed to be uniaxial, since it shows an easy direction and a hard direction of magnetization. The hysteresis loops associated with the easy and hard axes are similar to those of Co/Cu and are not shown here. The  $H_c$  value ranges from  $(6.93 \pm 0.24) \times 10^{-4} \text{ T}$  to  $(1.36 \pm 0.33) \times 10^{-4} \text{ T}$  and the squareness value varies from  $0.81 \pm 0.04$  to  $0.19 \pm 0.09$ . Our  $H_c$  value is about one order of magnitude lower than that of similar Co thickness (0.8 nm) and Al thickness (2.4 nm) in the Co/Al superlattice grown by magnetron sputtering reported in the literature [14].

Under the same experimental condition, the Kerr intensity and coercivity of the Co/Al superlattice are weaker than those of the Co/Cu superlattice. We have several reasons to explain this trend. First the RMS obtained from the AFM images indicates that the RMS of the Co/Al superlattice is larger than that of the Co/Cu superlattice. The roughness increases the thickness of the dead layer, typically slightly over 1 ML [25]. Secondly, the X-ray reflectivity shows that the interfacial roughness in the Co/Al superlattice is larger than that in Co/Cu. Thirdly, the Co alloys with the spacer layer such as Al to form the nonmagnetic CoAl alloy compounds at the interfaces of Co/Al superlattice. This effectively reduce the total amount of the pure Co layer that contributes to the Kerr intensity. For coercivity it depends on the films thickness [25]. In a few ML regime, the coercivity decreases as the Co film thickness reduces.

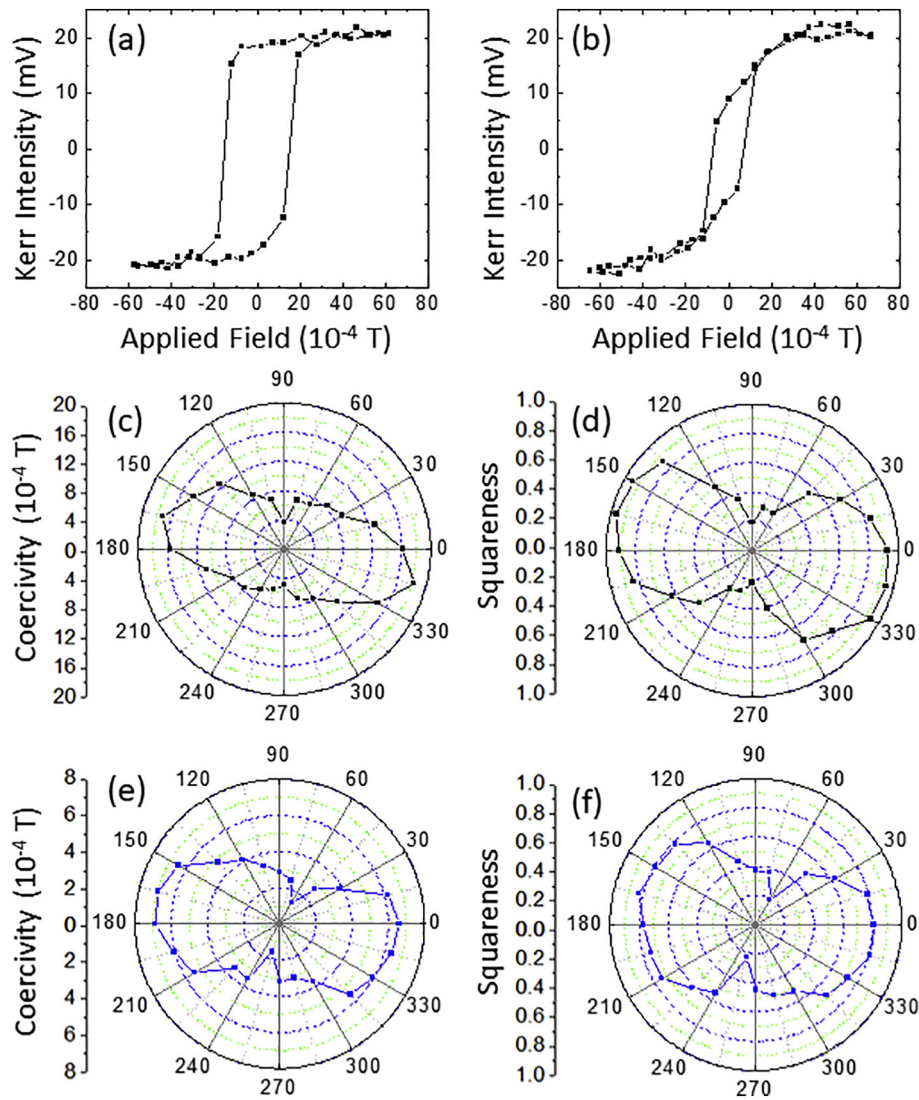


**Fig. 3.** Representative hysteresis loops of the Cu/Co superlattice thin film with the applied in-plane magnetic field along the (a) easy axis direction and (b) hard axis direction, measured by the longitudinal SMOKE technique. Polar plot of (c) coercivity and (d) squareness of the Co/Cu superlattice. Polar plot of (e) coercivity and (f) squareness of the Co/Al superlattice. Each polar plot is a function of the in-plane azimuthal angle from  $0^\circ$  to  $360^\circ$  with  $15^\circ$  increment. The distance in the radius of a polar plot represents the value of either the coercivity in (c) and (e) or squareness in (d) and (f).

The coercivity is related to the magnetic domain wall energy which contains a term related to the product of thickness and effective magnetization. Due to the formation of Co and Al alloy, the CoAl alloy region reduces the effective thickness and effective magnetization of Co. Therefore, the coercivity reduces in the Co/Al superlattice. All these factors, including the larger interfacial roughness, magnetic dead layer, nonmagnetic alloy compounds, reduced amount of Co and thinner Co layer in the Co/Al superlattice, contribute to a lower Kerr intensity and lower coercivity compared to those of the Co/Cu superlattice.

### 3.4. Possible origins of in-plane uniaxial anisotropy

The magnetic anisotropy of an epitaxial film typically grown on a single crystal substrate could originate from several sources: the magnetocrystalline anisotropy arising from spin-orbit coupling correlated to the crystalline structure of the epitaxial film; shape anisotropy from long range dipolar interactions; and magnetoelastic anisotropy from the strain in an epitaxial film. For the highly symmetric single crystalline film on single crystal substrate, one expects no in-plane uniaxial anisotropy. But exceptions do occur, for examples, with an epitaxial Fe (001) film grown on GaAs(001) [27] and a crystalline Fe film on Ge

buffered GaAs(001) [28]. Our superlattice is a polycrystalline film grown on amorphous  $\text{SiO}_2$  where the above-mentioned origins still could exist, but their anisotropies are random and challenging to differentiate. For polycrystalline films, the direction of the anisotropy depends on extrinsic factors such as substrate shape, surface step direction, and substrate treatment effects like surface polishing [29]. Here our substrate has a symmetrically square shape, see the right inset in Fig. 4(a), and the substrate is amorphous  $\text{SiO}_2$  with no polishing or steps before the growth of the superlattices. The anisotropy in the polycrystalline film could also come from the deposition effects, such as the obliqueness of the deposition [30–32] or annealing. In our superlattice growth the sputter target had a normal incidence on the substrate. If one considers the case when the shutter was first opened to expose the incident flux to the substrate, the estimated incident flux angle is  $\sim 14^\circ$  relative to the surface normal. This angle is not very oblique and may not introduce an obvious uniaxial anisotropy [30,32]. Recall that during the superlattice deposition, a very small DC  $1\ \mu\text{A}$  current was applied to the two Ta pads in the substrate. This  $1\ \mu\text{A}$  current produces negligible Joule heating during growth as indicated by the thermocouple readings. Besides, the superlattice sample was grown on a thermally conductive  $\text{SiO}_2/\text{Si}$  substrate. After the

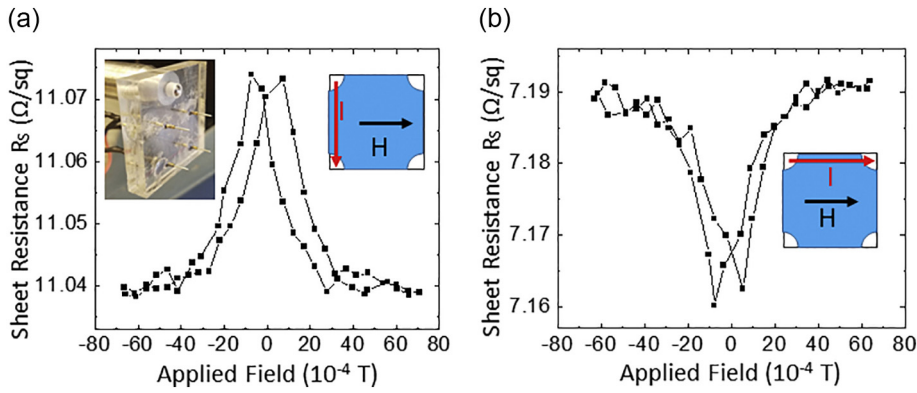


Fig. 4. Anisotropic sheet resistance of the Co/Cu superlattice vs. applied in-plane magnetic field when the applied current  $I$  is (a) perpendicular or (b) parallel to the applied in-plane magnetic field  $H$  (sweeping in the horizontal direction or along the azimuthal angle  $\phi = 180^\circ$  to  $0^\circ$ ). The left inset in (a) is a photo of the assembled four spring-loaded probes mounted on an acrylic plate.

superlattice was grown, the sample with the  $1 \mu\text{A}$  current still on was annealed to  $300^\circ\text{C}$  and then cooled down slowly to room temperature. The resistance measured at  $250^\circ\text{C}$  during cool down along the current edge decreased by  $4.3 \Omega$  compared to that before annealing, and the resistance along the voltage edge increased by  $2.7 \Omega$  compared to that before annealing. The decrease of resistance along the current applying edge suggests more grain growth. At the voltage edge, the current is much smaller than  $1 \mu\text{A}$  and the increase resistance is due to the higher temperature ( $250^\circ\text{C}$ ). These opposite resistance changes after film annealing indicates more grain growth where the current is higher. In reality, the current flow pattern is denser between and near the two electrodes where the current is applied [33] in comparison to that between electrodes where the voltage is measured. This current density gradient is uniaxial in the film, which results in uniaxial grain growth and most likely leads to the corresponding anisotropy in magnetic behavior.

For the polar SMOKE condition, we did not observe any hysteresis loop from either Co/Cu or Co/Al superlattice. For the Co/Al superlattice a gradual transition from out-of-plane to in-plane magnetization was reported when the Co thickness ranges from  $0.7 \text{ nm}$  to  $1.0 \text{ nm}$  [14]. We did not observe the out-of-plane magnetization in our superlattice because our Co thickness of  $0.8 \text{ nm}$  is at the threshold for where the out-of-plane transition occurs. We speculate that the same may be true for the Co/Cu superlattice.

### 3.5. Anisotropic magnetoresistance

The MR behavior originates from the Co's spin-dependent transmission of the conduction electrons through the Cu or Al spacer layers. The Montgomery method [33,34] (an extension of van der Pauw method [35]) for anisotropic film was employed where the four spring-loaded probes were made to contact the four Ta pads  $90^\circ$  apart at the circumference of the Co/Cu superlattice for a square four-point probe configuration. See the left inset of Fig. 4(a). The sheet resistances vs. the applied magnetic field strengths were measured as shown in Fig. 4(a) and (b), for the magnetic field perpendicular and parallel to the current, respectively. We used the conventional definition of  $\text{MR}\% = [R(H) - R(\text{Sat})]/R(\text{Sat})$ , where  $R(H)$  is the resistance at the peaks near the zero applied magnetic field and  $R(\text{Sat})$  is the resistance at the saturation field level, which is when the resistance levels off and does not change. It is noted that the observed saturation magnetic field is  $< 100 \times 10^{-4} \text{ T}$ . This is much lower than that observed in many superlattices with much higher number of repeated bilayer, for example,  $[\text{Co}(1 \text{ nm})/\text{Cu}(0.9 \text{ nm})]_{16}$  capped by  $5 \text{ nm}$  Cu and  $5 \text{ nm}$  Co [3]. Note that when the applied magnetic field is perpendicular to the applied current direction, the  $R(H) > R(\text{Sat})$  and the transverse MR has a positive value. When the applied magnetic field is parallel to the current passing direction, however,  $R(H) < R(\text{Sat})$  and the longitudinal MR value is negative. This phenomenon is known as the anisotropic magnetoresistance (AMR). This result is consistent with  $100 \text{ nm}$  thick  $[\text{Co}(1 \text{ nm})/\text{Cu}$

( $5 \text{ nm}$ )] multilayer grown by evaporation [36], sputtered deposited  $100 \text{ nm}$  thick polycrystalline Fe, Co, Ni and Ni alloyed films [37], and  $20 \text{ nm}$  thick nanogranular Co and Cu film alloy grown by co-evaporation of Co and Cu [15]. The two peaks observed in the resistance are near the coercivity field  $H_c$  shown in Fig. 3(a). The MR values extracted from over 10 measurements are  $+0.45 \pm 0.08\%$  and  $-0.49 \pm 0.04\%$  for the applied magnetic field perpendicular and parallel to the current passing direction, respectively. Note that the sample mounting position with azimuthal angle  $\phi = 0^\circ$  in the gap of electromagnet is along the horizontal direction for the measurement of hysteresis loop shown in Fig. 3(a). The sample position is the same as in the MR measurement in Fig. 4(b). This means that the measured negative MR is within  $15^\circ$  of the easy axis direction of the uniaxial anisotropy. The MR decreases as the film thickness decreases due to a higher percentage of interface scattering and grain boundaries scattering. In principle, if the film thickness of the three-bilayer is doubled, then the MR could increase to over  $1\%$ . The MR value in the Co/Al superlattice is within the noise level (not shown here) due to a larger interfacial roughness and possibly thinner pure Co layer as compared with that of the Co/Cu superlattice. Furthermore, the sheet resistance of Co/Al is higher than that of Co/Cu. For a small change in the numerator,  $R(H) - R(\text{Sat})$ , over a large resistance,  $R(\text{Sat})$ , in the denominator, the MR ratio is small in both scenarios.

The positive and negative MR or AMR can be qualitatively understood as follows. The AMR is the property of the material in which the electrical resistance depends on the angle between the direction of electric current ( $j$ ) and the direction of magnetization ( $M$ ). If magnetic moments exist in the material, then the electric current will be scattered by the magnetic moments. Because the scattering cross-section is the largest when  $M$  is parallel to  $j$  and becomes the smallest when they are perpendicular [38], one obtains  $R_{\parallel} > R_{\perp}$ , where  $R_{\parallel}$  and  $R_{\perp}$  represent the resistance measured under the longitudinal and transverse configurations, respectively. If no magnetic moments exist in the material, then the orientation of individual spins will be random. The resistivity  $R_0$  at  $M = 0$  is therefore between  $R_{\parallel}$  and  $R_{\perp}$ , or  $R_{\parallel} > R_0 > R_{\perp}$ . For a polycrystalline material, this angle-dependent resistance is described using the following formula:  $R(\theta) = R_{\perp} + (R_{\parallel} - R_{\perp})\cos^2\theta$ , where  $\theta$  is the angle between  $M$  and  $j$ . Note that literature uses the resistivity,  $\rho$ , instead of the resistance,  $R$ . The resistance can be converted to resistivity after the probes' geometrical factors for measurement are considered [33]. Therefore,  $\rho(\theta) = \rho_{\perp} + (\rho_{\parallel} - \rho_{\perp})\cos^2\theta = \rho_{\perp} + \Delta \rho \cos^2\theta$ . If we choose the resistance  $\rho_0$  at  $M = 0$  (or  $H = H_c$  in the hysteresis loop) as a reference, then the magnetoresistance  $(\rho_0 - \rho(H))/\rho(H)$  would be positive under transverse MR (because  $\rho_0 > \rho_{\perp}$ ) and negative under longitudinal MR (because  $\rho_{\parallel} > \rho_0$ ).  $\Delta \rho/\rho_{\parallel}$  is named magnetoresistive coefficient and is a parameter for a magnetoresistive sensor device [39]. The  $\Delta \rho/\rho_{\parallel}$  of permalloy  $\text{Ni}_x\text{Fe}_{1-x}$  film used in commercial magnetic angle sensor has a range of a few percent [40,41]. Using our sheet resistance data shown in Fig. 4 and that  $\rho$  is proportional to  $R$  [33], we obtained  $\Delta \rho/\rho_{\parallel}$  of  $\sim 53\%$  for Co/Cu superlattice.

Materials that exhibit AMR have applications in many areas such as automobile and consumer electronics. One example is the real time monitoring of moving directions such as in mobile phone and three-axis magnetometer [42]. This is because the AMR sensors can detect changes in magnetic fields created by moving objects.

#### 4. Conclusion

The magnetic and structural properties of three-bilayer Co/Cu and Co/Al superlattices grown on amorphous substrates by sputter deposition were presented. Both the Co/Cu and Co/Al superlattices have square-like longitudinal hysteresis loops with a soft coercivity of  $< 17 \times 10^{-4} \text{ T}$  and  $7 \times 10^{-4} \text{ T}$ , respectively, indicating the existence of a ferromagnetic coupling between the Co layers. For the Co/Cu and Co/Al superlattices, a uniaxial, in-plane anisotropy of the coercivity and squareness was observed, thus indicating the existence of the easy and hard axes in the sample plane. This uniaxial anisotropy may be induced by the preferred grain growth along the small probe current applied to the film for the *in-situ* resistivity monitoring during the post growth annealing at 300 °C. The Co/Cu superlattice also shows a room temperature anisotropic MR or AMR of about  $\pm 0.5\%$  with a positive value or a negative value depending on whether the applied current is perpendicular or parallel to the applied in-plane magnetic field, respectively. For the Co/Cu superlattice, the easy axis and hard axis directions are within 15° of the negative and positive MR directions, respectively. From the different degrees of interfacial roughness and nonmagnetic CoAl alloying at the interface, we found that the Co/Cu superlattice has more easily observable magnetic properties such as MR, than the Co/Al superlattice. The MR and  $H_c$  values could be increased if the Cu spacer layer thickness is grown to the optimal antiferromagnetic coupling thickness of 0.8 nm. The low coercivity and AMR observed in the three-bilayer Co/Cu superlattice, which has a total thickness of  $\sim 7 \text{ nm}$ , can be applied in low field sensors and transformer cores [43]. Current commercial magnetic angle sensor made of permalloy thin film using AMR effect have some key features. For examples, (1) It can sense the magnetic field direction independently for applied field strengths  $> 25 \text{ kA/m}$  ( $= 314 \times 10^{-4} \text{ T}$ ). (2) It is stable up to 150 °C ambient temperature, and (3) The film thickness is  $\sim 15 \mu\text{m}$  [39]. Our three-bilayer superlattices have improved material parameters. (1) The low coercivity of superlattice ( $\sim 17 \times 10^{-4} \text{ T}$ ) that allows the minimum magnetic field strength to be detected by one order of magnitude lower. The low saturation magnetic field observed in MR results in an increase of the  $dR/dH$  slope which is preferable in magnetic sensor applications [41]. (2) The AMR was measured from the superlattice after annealing to 300 °C followed by cooling down to room temperature. This means the sensor made of the superlattice is stable up to 300 °C. (3) Since our superlattice is ultrathin, the sensor can be made very thin that can fit in a tight space. The fabrication process would involve fewer materials and, therefore, become more cost effective. In addition, the ultrathin superlattices could be grown on flexible membrane substrates such as Si and fabricated into flexible sensors.

#### Acknowledgement

This work is supported by the New York State Foundation of Science, Technology and Innovation (NYSTAR) through Focus Center-New York C150117, NSF REU DMR-1560266, SUNY and Rensselaer. We acknowledge the discussions with T.-M. Lu, P. Nawarat, J.Z. Lin, and Jiali Cheng. We also thank John Szczesniak for his help in laser drilling four holes at the corners of a square shape acryl plate for mounting the four-point probes. We also thank J. Z. Sun of IBM Thomas J. Watson Research Center for support and assistance in superlattice growth.

#### References

- [1] I.K. Schuller, S. Kim, C. Leighton, Magnetic superlattices and multilayers, *J. Magnet. Mater.* 200 (1999) 571.
- [2] S.S.P. Parkin, N. More, K.P. Roche, Oscillations in exchange coupling and magnetoresistance in metallic superlattice structures: Co/Ru, Co/Cr, and Fe/Cr, *Phys. Rev. Lett.* 64 (1990) 2304.
- [3] S.S.P. Parkin, Z.G. Li, D.J. Smith, Giant magnetoresistance in antiferromagnetic Co/Cu multilayers, *Appl. Phys. Lett.* 58 (23) (1991) 2710.
- [4] D.H. Mosca, F. Petroff, A. Fert, P.A. Schroeder, W.P. Pratt, R. Laloe, Oscillatory interlayer coupling and giant magnetoresistance in Co/Cu multilayers, *J. Magn. Mater.* 94 (1) (1991) L1.
- [5] Z.J. Yang, M.R. Scheinfein, Interfacial-roughness effects on giant magnetoresistance and interlayer coupling in Co/Cu superlattices, *Phys. Rev. B* 52 (6) (1995) 4263.
- [6] Z.J. Yang, M.R. Scheinfein, 90° domains in Co/Cu giant magnetoresistance superlattices, *Appl. Phys. Lett.* 66 (2) (1995) 236.
- [7] L.A. Chebotkevich, Y.D. Vorobev, A.S. Samardak, A.V. Ognev, Effect of the crystal structure and interlayer exchange coupling on the coercive force in Co/Cu/Co films, *Phys. Solid State* 45 (5) (2003) 907.
- [8] M.N. Baibich, J.M. Broto, A. Fert, F.N. Van Dau, F. Petroff, P. Etienne, G. Creuzet, A. Friederich, J. Chazelas, Giant magnetoresistance of (001)Fe/(001)Cr magnetic superlattices, *Phys. Rev. Lett.* 61 (21) (1988) 2472.
- [9] D. BANG, H. AWANO, Y. SAITO, J. TOMINAGA, Magnetic Field-dependent magneto-optical Kerr effect in [(GeTe)<sub>2</sub>(Sb<sub>2</sub>Te<sub>3</sub>)<sub>1</sub>]<sub>n</sub> topological superlattice, *J. Electron. Mater.* 45 (5) (2016) 2496.
- [10] T. Gu, A.I. Goldman, M. Mao, Characterization of interfacial roughness in Co/Cu multilayers by X-ray scattering, *Phys. Rev. B* 56 (11) (1997) 6474.
- [11] A. de Bernabe, M.J. Capitan, H.E. Fischer, C. Prieto, Study of interfaces in Co/Cu multilayers by low-angle anomalous X-ray diffraction, *J. Appl. Phys.* 84 (4) (1998) 1881.
- [12] J.D. Kim, A.K. Petford-Long, J.P. Jakubovics, J.E. Evetts, R. Somekh, Structure and magnetic properties of Co/Cu multilayer films, *J. Appl. Phys.* 76 (4) (1994) 2387.
- [13] T. Mitsuoka, A. Kamijo, H. Igarashi, Structure and magnetic properties of Co/Al multilayered films, *J. Appl. Phys.* 68 (4) (1990) 1787.
- [14] F.Z. Cui, J.F. Wang, Y.D. Fan, H.D. Li, Magnetic CoAl multilayers prepared by planar magnetron sputtering, *J. Appl. Phys.* 70 (6) (1991) 3379.
- [15] I.O. Shpetnyi, D.M. Kondrakhova, S.I. Vorobiov, B. Scheibe, V.I. Grebinaha, D.O. Derecha, Y.I. Gorobets, I.Y. Protchenko, The structural-phase state and magnetoresistive properties of thin film alloys obtained by co-evaporated Cu and Co, *J. Magn. Mater.* 474 (2019) 624.
- [16] E.R. Moog, S.D. Bader, Smoke signals from ferromagnetic monolayers: p(1 × 1) Fe/Au(100), *Superlattice. Microst.* 1 (1985) 543.
- [17] Z.Q. Qiu, S.D. Bader, Surface magneto-optic Kerr effect, *Rev. Sci. Instrum.* 71 (3) (2000) 1243.
- [18] J.P. Qian, G.-C. Wang, A simple ultrahigh vacuum surface magneto-optic Kerr effect setup for the study of surface magnetic anisotropy, *J. Vac. Sci. Technol. A* 8 (1990) 4117.
- [19] M. Li, G.-C. Wang, A setup combining four-point probe and surface magneto-optical Kerr effect for measurements of magnetotransport and magnetic properties of ultrathin films in ultrahigh vacuum, *Rev. Sci. Instrum.* 69 (1998) 1811.
- [20] H.N. Yang, G.-C. Wang, T.-M. Lu, Diffraction From Rough Surfaces and Dynamic Growth Fronts, World Scientific, 1993.
- [21] Y.-P. Zhao, G.-C. Wang, T.-M. Lu, Characterization of amorphous and crystalline rough surface: principles and applications, *Experimental Methods in the Physical Science*, 37 Academic Press, 2001.
- [22] S.A. Chuprakov, T.P. Krinitsina, N.S. Bannikova, I.V. Blinov, S.V. Verkhovskii, M.A. Milyaev, V.V. Popov, V.V. Ustinov, Interface structure and magnetoresistance studies of [Co/Cu]<sub>n</sub> superlattices by means of NMR and TEM, *Solid State Phenom.* 215 (2014) 358.
- [23] A. de Bernabe, M.J. Capita, H.E. Fischer, S. Lequien, F.J. Mompea, C. Prieto, C. Quiro, J. Colino, S. Lefebvre, M. Bessie, J.M. Sanz, Oxidation study of Co/Cu multilayers by resonant X-ray reflectivity, *Vacuum* 52 (1999) 109.
- [24] P. Hansen, Constitution of Binary Alloys, McGraw-Hill, NY (1958), p. 79.
- [25] Q. Jiang, H.-N. Yang, G.-C. Wang, Effect of interface roughness on hysteresis loops of ultrathin Co films from 2 ML to 30 ML on Cu(001) surfaces, *Surf. Sci.* 373 (1997) 181.
- [26] J. Camarero, J.J. de Miguel, R. Miranda, A. Hernando, Thickness-dependent coercivity of ultrathin Co films grown on Cu(111), *J. Phys. Condens. Matter* 12 (2000) 7713.
- [27] M. Zolfi, M. Brockmann, M. Kohler, S. Kreuzer, T. Schweinbock, S. Miethaner, F. Bensch, G. Bayreuther, Magnetic films epitaxially grown on semiconductors, *J. Mag. Mater.* 175 (1997) 16.
- [28] S.-K. Bac, H. Lee, S. Lee, S. Choi, Y. Taehee, S. Lee, X. Liu, J.K. Furdyna, Observation of uniaxial anisotropy along the [100] direction in crystalline Fe film, *Sci. Rep.* 5 (17761) (2015) 1.
- [29] J.B. Wedding, M. Li, G.-C. Wang, Magnetization reversal of a thin polycrystalline cobalt film measured by the magneto-optic Kerr effect (MOKE) technique and field-dependent magnetic force microscopy, *J. Magn. Mater.* 204 (1999) 79.
- [30] T. Tang, D.-L. Liu, D.-X. Ye, T.-M. Lu, G.-C. Wang, Asymmetry of magneto-optical Kerr effect loops of Co nano-columns grown by oblique incident angle deposition, *J. Magn. Mater.* 283 (2004) 65.
- [31] P. Morrow, X.-T. Tang, T.C. Parker, M. Shima, G.-C. Wang, Magnetoresistance of oblique angle deposited multilayered Co/Cu nanocolumns measured by a scanning tunnelling microscope, *Nanotechnology* 19 (9) (2008) 065712.
- [32] J.H. Wolfe, R.K. Kawakami, W.L. Ling, Z.Q. Qiu, R. Arias, D.L. Mills, Roughness

- induced in plane uniaxial anisotropy in ultrathin Fe films, *J. Magn. Magn. Mater.* 232 (1) (2001) 36.
- [33] I. Miccoli, F. Edler, H. Pfnur, C. Tegenkamp, The 100th anniversary of the four-point probe techniques: the role of probe geometries in isotropic and anisotropic systems, *J. Phys. Condens. Matter* 27 (2015) 223201.
- [34] H.C. Montgomery, Method for measuring electrical resistivity of anisotropic materials, *J. Appl. Phys.* 42 (7) (1971) 2971.
- [35] I.J. van der Pauw, Method of measuring specific resistivity and hall effect of disk of arbitrary shape, *Philips Res. Rep.* 13 (1958) 1.
- [36] S. Zsuzsa, L. Péter, L.F. Kiss, I. Bakonyi, Magnetic and magnetoresistance studies of nanometric electrodeposited Co films and Co/Cu layered structures: Influence of magnetic layer thickness, *J. Magn. Magn. Mater.* 421 (2017) 194.
- [37] S.S.P. Parkin, Giant magnetoresistance and oscillatory interlayer coupling in polycrystalline transition metal multilayers, in: B. Heinrich, J.A.C. Bland (Eds.), *Ultrathin Magnetic Structures II*, Springer-Verlag Berlin Heidelberg, 1994, p. 156.
- [38] T.R. McGuire, R.I. Potter, Anisotropic magnetoresistance in ferromagnetic 3d alloys, *IEEE Trans. Magnet. MAG* 11 (4) (1975) 1018.
- [39] L. Jogschies, D. Klaas, R. Kruppe, J. Rittinger, P. Taptimthong, A. Wienecke, L. Rissing, M.C. Wurz, Recent developments of magnetoresistive sensors for industrial applications, *Sensors (Basel, Switzerland)* 15 (/11) (2015) 28665.
- [40] W. Kwiatkowski, S. Tumanski, The permalloy magnetoresistive sensors-properties and applications, *J. Phys. E* 19 (7) (1986) 502.
- [41] J. Heremans, Solid state magnetic field sensors and applications, *J. Phys. D. Appl. Phys.* 26 (8) (1993) 1149.
- [42] V.-T. Pham, D.-C. Nguyen, Q.-H. Tran, D.-T. Chu, D.-T. Tran, Thermal stability of magnetic compass sensor for high accuracy positioning applications, *Sens. Trans. J.* 195 (/12) (2015) 1.
- [43] O. Gutfleisch, M.A. Willard, E. Bruck, C.H. Chen, S.G. Sankar, J.P. Liu, Magnetic materials and devices for the 21st century: stronger, lighter, and more energy efficient, *Adv. Mater.* 23 (2011) 821.